#### THE FORMATION AND DYNAMICAL EVOLUTION OF YOUNG STAR CLUSTERS

M. S. Fujii<sup>1</sup> Division of Theoretical Astronomy, National Astronomical Observatory of Japan, 2–21–1 Osawa, Mitaka, Tokyo 181–8588

S. PORTEGIES ZWART<sup>2</sup>
Leiden Observatory, Leiden University, PO Box 9513, 2300 RA, Leiden, The Netherlands michiko.fujii@nao.ac.jp

Draft version December 2, 2015

#### ABSTRACT

Recent observations have revealed a variety of young star clusters, including embedded systems, young massive clusters, and associations. We study the formation and dynamical evolution of these clusters using a combination of simulations and theoretical models. Our simulations start with a turbulent molecular cloud that collapses under its own gravity. The stars are assumed to form in the densest regions in the collapsing cloud after an initial free-fall times of the molecular cloud. The dynamical evolution of these stellar distributions are continued by means of direct N-body simulations. The molecular clouds typical for the Milky Way Galaxy tend to form embedded clusters which evolve to resemble open clusters. The associations were initially considerably more clumpy, but lost their irregularity in about a dynamical time scale due to the relaxation process. The densest molecular clouds, which are absent in the Milky Way but are typical in starburst galaxies, form massive young star clusters. They indeed are rare in the Milky Way. Our models indicate a distinct evolutionary path from molecular clouds to open clusters and associations or to massive star clusters. The mass-radius relation for both types of evolutionary tracks excellently matches the observations. According to our calculations the time evolution of the half-mass radius for open clusters and associations follows  $r_h/pc = 2.7(t_{age}/pc)^{2/3}$ , whereas for massive star clusters  $r_{\rm h}/{\rm pc} = 0.34 (t_{\rm age}/{\rm Myr})^{2/3}$ . Both trends are consistent with the observed age-mass-radius relation for clusters in the Milky Way.

Subject headings: galaxies: star clusters: general — (Galaxy:) open clusters and associations: general — methods: numerical

#### 1. INTRODUCTION

Star clusters are classically categorized in two groups, Galactic open clusters and globular clusters. Open clusters are generally rather young ( $\lesssim 1\,\mathrm{Gyr}$ ) with typically  $100-10^4$  stars, hereafter we call them "classical" open clusters. Globular clusters are old ( $\gtrsim 10\,\mathrm{Gyr}$ ), more massive ( $\gtrsim 10^5 M_{\odot}$ ), and dense ( $\gtrsim 100 M_{\odot} \mathrm{pc}^{-3}$ ). Recent observations indicate that there is a wide variety among open star clusters in the Milky Way. These types include

- embedded clusters, which are very young  $\lesssim 3$  Myr and therefore still embedded in their natal gas cloud (Lada & Lada 2003). Embedded clusters reside in the Galactic disk and are composed of several 100 stars in a volume with a radius of  $\sim 1$  pc (Figuerêdo et al. 2002).
- associations, which are considered unbound from the moment they were born (Gieles & Portegies Zwart 2011).
- massive clusters, which are also young ( $\lesssim 10$  Myr) and extremely dense ( $\gtrsim 10^3 M_{\odot} {\rm pc}^{-3}$ ) (Portegies Zwart et al. 2010).

Some of embedded clusters evolve into classical open clusters, if they survive gas expulsion (Lada & Lada 2003; Fujii 2015a).

Young massive clusters are common in nearby starburst galaxies such as in M83 (Bastian et al. 2011) and M51

(Chandar et al. 2011), but they are rare in the Milky Way. Two massive young star clusters reside close to the Galactic center, i.e., Arches and Quintuplet, and the others are in the spiral arms. This latter category includes the clusters NGC 3603, Westerlund 1 and 2, and Trumpler 14 (Portegies Zwart et al. 2010).

Pfalzner (2009) suggested another type of young star clusters, "leaky clusters." Leaky clusters have a mass similar to those of the massive clusters ( $\sim 10^4 M_{\odot}$ ), but with a much lower density ( $\sim 1-10 M_{\odot} \mathrm{pc}^{-3}$ ). Portegies Zwart et al. (2010) classified the leaky clusters listed in Pfalzner (2009) as OB associations.

According to the argumentation in Gieles & Portegies Zwart (2011) the distinction between an open cluster and an association can be made on the ratio between the age of the stars and dynamical time of the system  $(t_{\rm age}/t_{\rm dyn})$ . If the age of the stars exceed the dynamical age of the system, the stars must be bound together. Otherwise the system is unbound.

In an attempt to clarify the various classes and families of stellar conglomerates we discuss, in this paper, the formation and dynamical evolution of young star clusters by means of simulations. The numerical modeling used here allows us to make a more clear distinction between the difference in initial conditions and the difference in evolution. It therefore helps us to differentiate between the various classes and families of clustered stellar environments.

<sup>&</sup>lt;sup>1</sup> NAOJ Fellow

In previous papers, we performed direct N-body simulations using initial conditions constructed from the results of hydrodynamical simulations of turbulent molecular clouds. There we found that young massive clusters form from turbulent molecular clouds, if the local star formation efficiency depends on the local gas density (Fujii & Portegies Zwart 2015; Fujii 2015b). We also found that observed embedded clusters tend to evolve into classical open clusters (Fujii 2015b). Our simulations, however, did not provide a channel for forming associations (or leaky clusters, according to Pfalzner (2009)).

At this point it is still unclear how leaky clusters form. Pfalzner (2011) proposed that leaky clusters are born as embedded clusters, that their mass increases due to a prolonged phase of star formation, and that the expansion is driven by the expulsion of the residual gas. This scenario was tested by means of simulations in Pfalzner & Kaczmarek (2013), Parmentier & Pfalzner (2013), and Pfalzner et al. (2014), in which it was concluded that the known embedded clusters in the Galactic disk are the ancestors of leaky clusters.

In our previous simulations we did not find leaky clusters. This may have been a result of our selected initial conditions for the parental molecular cloud, for which we chose rather massive  $(10^5-10^6\,M_\odot)$  and dense  $(100-1000\,\mathrm{cm}^{-3})$  structures. The molecular clouds observed in the Milky Way tend to follow Larson's relation (Larson 1981), which indicates a relation between cloud mass and density: According to this law massive clouds have a lower density, if the clouds are close to be virialized. The initial conditions in our previous study would then biased towards too dense clouds compared to the typical massive clouds in the Milky Way.

In this paper, we expand on the initial parameter space, by also allowing massive clouds with a lower density. This expansion of the parameter space helps in the formation of associations, as well as for making dense massive clusters. We support our numerical models with theoretical arguments in order to understand the the dynamical evolution of each type of star clusters (classical open, embedded, young massive, and leaky clusters or associations).

#### 2. SIMULATIONS

We perform a series of N-body simulations based on the results of hydrodynamical simulations of turbulent molecular clouds. We first perform simulations of molecular clouds with a turbulent velocity field using an smoothed particle hydrodynamics (SPH) code. The resolution of the hydrodynamical simulations is relatively low and therefore the simulation cannot resolve the formation of individual stars, but can resolve the clumpy structures of the gas. After around one free-fall time of the initial molecular clouds, we stop the hydrodynamical simulations and replace a part of gas particles with stellar particles assuming a star formation efficiency depending on the local density. We then remove all residual gas particles and perform direct Nbody simulations only with stellar particles. We describe the details of the initial conditions and the simulations in the following (see also Fujii & Portegies Zwart 2015; Fujii 2015b).

#### 2.1. The Astronomical Multipurpose Software Environment

The hydrodynamical simulations and the data analyses in this study are performed using the AMUSE framework (Portegies Zwart et al. 2013; Pelupessy et al. 2013). AMUSE is not a single code, but a extensive library of more than 50 high-performance simulation codes. The AMUSE consortium is a spin-off from the MODEST community, which upon three workshop in Lund, Amsterdam, and Split culminated in a first implementation of, what at that time was called the Multi-User Software Environment (or MUSE) (Portegies Zwart et al. 2009). Later the package was extended from its primary objective of Noah's Arc (two codes per domain) to about a dozen codes per domain.

Apart from scientific production software, AMUSE also supports from generating initial conditions to data processing. The fundamental package is written in the Python language and it is freely available via Github and via the project web page at http://amusecode.org. All the scripts used to run the simulations in this paper are available via this project web page.

#### 2.2. Hydrodynamical Simulations

### 2.2.1. Initial Conditions for Molecular Clouds

All initial conditions are generated using the AMUSE framework. We adopt isothermal (30K) homogeneous spheres as initial conditions of molecular clouds following Bonnell et al. (2003). We give a divergence-free random Gaussian velocity field  $\delta v$  with a power spectrum  $|\delta v|^2 \propto k^{-4}$  (Ostriker et al. 2001; Bonnell et al. 2003). The spectral index of -4 appears in the case of compressive turbulence (Burgers turbulence), and recent observations of molecular clouds (Heyer & Brunt 2004) and numerical simulations (Federrath et al. 2010; Roman-Duval et al. 2011; Federrath 2013a) also suggested values similar to -4. Each model is run with a different random seed for a realization of the initial conditions.

We adopt the virial ratio  $|E_{\rm k}|/|E_{\rm p}|=1$  (here  $E_{\rm k}$  and  $E_{\rm p}$  are kinetic and potential energies) and three masses for the molecular clouds of  $M_{\rm g}=10^4,\,4\times10^5,\,{\rm and}\,\,10^6\,M_{\odot}$ . The density of these molecular clouds are  $\rho_{\rm g}=17,\,170,\,{\rm and}\,\,1700\,{\rm cm}^{-3}$  (which corresponds to 1, 10, and 100  $M_{\odot}{\rm pc}^{-3}$  assuming that the mean weight per particle is  $2.33m_{\rm H},\,{\rm respectively}$ ). The initial conditions are summarized in Table 1.

Once we chose the cloud mass and density, the radius  $(R_{\rm g})$  and the velocity dispersion in three dimensions  $(\sigma_{\rm g})$  are determined. Some of our models (such as a models m1M-d1-s15, m1M-d1-s16 and m1M-d1-s17, with  $M_{\rm g}=10^6M_{\odot}$  and  $\rho_{\rm g}=17{\rm cm}^{-3})$  roughly follow Larson's relation (Larson 1981),

$$\sigma \sim \left(\frac{L}{1\text{pc}}\right)^{0.5} (\text{km s}^{-1}),\tag{1}$$

where  $\sigma$  is the velocity dispersion and L is the size of the cloud (Heyer & Brunt 2004; Mac Low & Klessen 2004).

In Figure 1 we present the distribution of mass and density for the simulations listed in Table 1. In order to determine the mass of a molecular cloud that is consistent with Larson's relation we adopt a velocity dispersion of

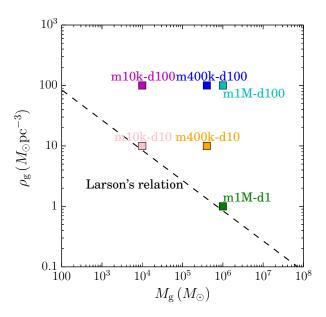


Fig. 1.— Mass-density relation of our initial models (see Table 1). The dashed line indicates the mass-density relation from Larson's relation (Larson 1981) for virialized cloud ( $\sigma_{\rm g}^2 = GM_{\rm g}/R_{\rm g}$ ).

Table 1 Initial conditions for the hydrodynamical simulations. All models are super virial, with  $|E_{\rm k}|/|E_{\rm p}|=1$ 

| Model         | Mass                  | Radius                | Density                              | Velocity dispersion               | Initial free-fall time    |
|---------------|-----------------------|-----------------------|--------------------------------------|-----------------------------------|---------------------------|
|               | $M_{ m g}(M_{\odot})$ | $r_{\rm g}~({ m pc})$ | $ ho_{\mathrm{g}}(\mathrm{cm}^{-3})$ | $\sigma_{\rm g}~({\rm kms^{-1}})$ | $t_{\rm ff,i}~({ m Myr})$ |
| m1M-d100-s7   | $1 \times 10^{6}$     | 13.4                  | $1.7 \times 10^{3}$                  | 19.6                              | 0.81                      |
| m1M-d1-s15    | $1 \times 10^{6}$     | 62                    | 17                                   | 9.1                               | 8.1                       |
| m1M-d1-s16    | $1 \times 10^{6}$     | 62                    | 17                                   | 9.1                               | 8.1                       |
| m1M-d1-s17    | $1 \times 10^{6}$     | 62                    | 17                                   | 9.1                               | 8.1                       |
| m400k-d100-s1 | $4 \times 10^5$       | 10                    | $1.7 \times 10^{3}$                  | 14.4                              | 0.82                      |
| m400k-d100-s2 | $4 \times 10^5$       | 10                    | $1.7 \times 10^{3}$                  | 14.4                              | 0.82                      |
| m400k-d100-s3 | $4 \times 10^5$       | 10                    | $1.7 \times 10^{3}$                  | 14.4                              | 0.82                      |
| m400k-d10-s8  | $4 \times 10^5$       | 21                    | 170                                  | 9.9                               | 2.5                       |
| m400k-d10-s9  | $4 \times 10^5$       | 21                    | 170                                  | 9.9                               | 2.5                       |
| m10k-d100-s4  | $1 \times 10^{4}$     | 2.87                  | $1.7 \times 10^{3}$                  | 4.2                               | 0.81                      |
| m10k-d100-s5  | $1 \times 10^4$       | 2.87                  | $1.7 \times 10^{3}$                  | 4.2                               | 0.81                      |
| m10k-d100-s6  | $1 \times 10^{4}$     | 2.87                  | $1.7 \times 10^{3}$                  | 4.2                               | 0.81                      |
| m10k-d10-s11  | $1 \times 10^4$       | 6.2                   | 170                                  | 2.9                               | 2.6                       |
| m10k-d10-s12  | $1 \times 10^{4}$     | 6.2                   | 170                                  | 2.9                               | 2.6                       |
| m10k-d10-s13  | $1 \times 10^4$       | 6.2                   | 170                                  | 2.9                               | 2.6                       |

<sup>&#</sup>x27;s' indicates the random seeds for the turbulence.

 $\sigma_{\rm g} \simeq \sqrt{GM_{\rm g}/R_{\rm g}}$ . Some models have initially a higher velocity dispersion, which we motivate through cloud-cloud collisions (Furukawa et al. 2009; Fukui et al. 2013, 2014) or to simulate molecular clouds in starburst galaxies. We further motivate and discuss on our choice of the initial conditions in  $\S$  4.

#### 2.2.2. Smoothed Particle Hydrodynamics Simulations

We perform hydrodynamical simulations using the SPH code Fi (Hernquist & Katz 1989; Gerritsen & Icke 1997; Pelupessy et al. 2004; Pelupessy 2005) in the AMUSE framework. Our calculations have relatively low mass resolution of  $m = 1 M_{\odot}$  per particle. The gravitational softening length during the hydrodynamical simulations is  $0.1\,\mathrm{pc}$ , and the SPH softening length (h) is chosen such that  $\rho_{\rm g}h^3 = mN_{\rm nb}$  (Springel & Hernquist 2002). Here  $N_{\rm nb} = 64$  is the target number of neighbor particles. With the adopted isothermal gas temperature of 30 K we can resolve the Jeans instability down to  $h \sim 0.4 \,\mathrm{pc}$ , which is smaller than the typical size of known embedded clusters (1 pc) (Lada & Lada 2003) but somewhat larger than the observed typical width of gas filaments ( $\sim 0.1 \text{ pc}$ ) (Arzoumanian et al. 2011). With these limitations, we obviously cannot resolve the formation of individual stars, but we do resolve dense gas clumps. We think that the limited resolution of our hydrodynamical simulations does not pose a serious problem, because we are interested in the global dynamical structure of the molecular cloud after only about an initial free-fall time scale,  $t_{\rm ff,i}$  (see Table 1 for the free fall time scales for each of the initial models). In fact, after  $0.9t_{\rm ff,i}$  we stop the hydrodynamical simulation to analyze the resulting gas distribution, initialize stars, and continue the simulations using a gravitational N-body code.

#### 2.3. The star formation

After stopping the hydrodynamical simulation (around  $\sim 0.9 t_{\rm ff,i}$ ) we replace some of the SPH particles with stellar particles. The selection of SPH particles is based, through the local gas density  $\rho$ , on the local star formation efficiency (SFE)  $\epsilon_{\rm loc}$ :

$$\epsilon_{\rm loc} = \alpha_{\rm sfe} \left( \frac{\rho}{100 \, M_{\odot} \text{pc}^{-3}} \right)^{0.5}. \tag{2}$$

Here  $\alpha_{\rm sfe}$  is a free parameter in our simulations to control the SFE. the form of  $\epsilon_{\rm loc}$  (Eq. 2) is motivated by the observations of individual molecular clouds for which the star formation rate is argued to scales with local free-fall time scale (Krumholz et al. 2012; Federrath 2013b).

Here we adopt  $\alpha_{\rm sfe}=0.02$ , which reproduces the observed global SFE across an entire molecular cloud of several per cent, but also leads to a 10–30% SFE in dense regions (>  $1000 M_{\odot} {\rm cm}^{-3}$ ) (Lada & Lada 2003; Higuchi et al. 2009; Federrath & Klessen 2013). In Table 2 we present the global SFE ( $\epsilon$ ) and the SFE for the dense regions ( $\epsilon_{\rm d}$ ) in our simulations.

Depending on the local SFE we replace individual gas particles to individual stellar particles conserving their positions and velocities. For each selected particle we assign a mass from the Salpeter mass function (Salpeter 1955) between  $0.3\,M_\odot$  and  $100M_\odot$ , irrespective of the mass of its parent SPH particle. The mean mass of the adopted

mass function is  $1 M_{\odot}$ , which corresponds to the mass of individual SPH particles. Mass in our simulations is therefore globally conserved, but not locally.

#### 2.4. N-body simulations

After the stellar particles are initialized (mass randomly from the Salpeter mass function, and position and velocity from the parent SPH particle), we remove the residual gas, leaving only the stellar particles in the simulations. The instantaneous removal of the gas has not a dramatic effect on the stellar distribution, because most stars are formed in the densest regions where little low-density (residual) gas is present. The gas that is insufficiently dense to form stars tend to be enveloping the densest stellar conglomerates.

We now switch on the N-body code, for which we adopted the direct sixth-order Hermite predictor-corrector scheme (Nitadori & Makino 2008) without gravitational softening and with an accuracy parameter,  $\eta = 0.1-0.25$ . The total energy error over the time span of the N-body simulations remained below  $\sim 10^{-3}$ .

The sizes of the stars we adopted from the zero-age main sequence radii for solar metallicity stars Hurley et al. (2000). We allow stars to collide using the sticky sphere approach. New stellar radii are assumed to be the zero-age main sequence radii for the new mass. Stellar mass-loss was incorporated only at the end of the main sequence Hurley et al. (2000) (see Fujii et al. 2009; Fujii & Portegies Zwart 2013, for the details).

We did not perform the N-body simulations for models m10k-d10 ( $M_{\rm g}=10^4M_{\odot}$  and  $\rho_{\rm g}=10M_{\odot}{\rm pc}^{-3}=170{\rm cm}^{-3}$ ), because the hydrodynamical simulations resulted in less than 100 stars and we aim at  $\gtrsim 100M_{\odot}$  star clusters. In these simulations even the densest regions were  $< 1000M_{\odot}{\rm pc}^{-3}$ .

#### 3. Results

# 3.1. Formation of Embedded, Classical Open, and Young Massive Clusters

The N-body simulations are started at what we will call  $t=0\,\mathrm{Myr}$ . The initial distribution of stars follows the distribution of the densest regions in the turbulent molecular cloud. In Figure 2 we present a time series of snapshots of model m400k-d100-s3. The entire system continuously expands because not all stars are bound after gas expulsion. The distribution of stars is clumpy and it takes a few Myr before the stars assemble in a more coherent aggregate.

We interrupt the simulations twice, at t=2 and at  $t=10\,\mathrm{Myr}$ , in order to analyze the stellar distribution, and detect clustered aggregates. Clumps are found in these snapshots by means of HOP (Eisenstein & Hut 1998) in AMUSE, using an outer cut-off density of  $\rho_{\mathrm{out}}=4.5M_{\mathrm{s}}/(4\pi R_{\mathrm{h}}^3)$  (three times the half-mass density of the entire stellar system,  $\rho_{\mathrm{h}}=M_{\mathrm{s}}/(8\pi R_{\mathrm{h}}^3)$ , where  $M_{\mathrm{s}}$  is the total stellar mass and  $R_{\mathrm{h}}$  is the half-mass radius of the entire distribution of the stars), a saddle-point density threshold ( $\rho_{\mathrm{saddle}}=8\rho_{\mathrm{out}}$ ) and the peak density threshold ( $\rho_{\mathrm{peak}}=10\rho_{\mathrm{out}}$ ) and the number of particles for neighbor search ( $N_{\mathrm{dense}}$ ) as well as the number of particles to calculate the local density ( $N_{\mathrm{hop}}$ ) are set to be 64. The number of neighbors is used to determine which two groups merge  $N_{\mathrm{merge}}=4$ . With these settings the detection limit of the

| Table 2 |     |        |             |  |  |  |  |  |
|---------|-----|--------|-------------|--|--|--|--|--|
| Models  | FOR | N-body | SIMULATIONS |  |  |  |  |  |

| Model            | Mass                  | N of particles | Virial ratio*                       | SFE (Global) | SFE (Dense)       |
|------------------|-----------------------|----------------|-------------------------------------|--------------|-------------------|
| Model            | $M_{ m s}(M_{\odot})$ | •              |                                     | ` ,          | ,                 |
| 13.5.11.00       | \ - /                 | $N_{ m s}$     | $ E_{\mathbf{k}} / E_{\mathbf{p}} $ | $\epsilon$   | $\epsilon_{ m d}$ |
| m1M-d100-s7      | $1.1 \times 10^{5}$   | 109080         | 0.9                                 | 0.11         | 0.27              |
| m1M-d1-s16       | $1.9 \times 10^{4}$   | 18760          | 0.50                                | 0.019        | 0.63              |
| m1M-d1-s16-t0.75 | $4.6 \times 10^{3}$   | 4566           | 19                                  | 0.0046       | 0.42              |
| m1M-d1-s16-t0.65 | $3.9 \times 10^{3}$   | 3855           | 131                                 | 0.0039       | 0.083             |
| m1M-d1-s15-t0.75 | $5.9 \times 10^{3}$   | 5902           | 1.6                                 | 0.0059       | 0.49              |
| m1M-d1-s15-t0.65 | $4.0 \times 10^{3}$   | 3954           | 80                                  | 0.0040       | 0.12              |
| m1M-d1-s17-t0.75 | $5.5 \times 10^3$     | 5506           | 6.4                                 | 0.0055       | 0.26              |
| m1M-d1-s17-t0.65 | $4.3 \times 10^{3}$   | 4322           | 63                                  | 0.0043       | 0.088             |
| m400k-d100-s1    | $3.2 \times 10^{4}$   | 31895          | 1.3                                 | 0.078        | 0.22              |
| m400k-d100-s2    | $2.3 \times 10^{4}$   | 23273          | 4.2                                 | 0.057        | 0.16              |
| m400k-d100-s3    | $4.3 \times 10^4$     | 42596          | 0.43                                | 0.096        | 0.25              |
| m400k-d10-s8     | $1.5 \times 10^{4}$   | 14978          | 1.4                                 | 0.037        | 0.38              |
| m400k-d10-s9     | $2.8 \times 10^{4}$   | 27891          | 0.41                                | 0.068        | 0.39              |
| m10k-d100-s4     | $4.1 \times 10^{2}$   | 406            | 5.9                                 | 0.042        | 0.11              |
| m10k-d100-s5     | $2.6 \times 10^{2}$   | 256            | 7.4                                 | 0.027        | 0.079             |
| m10k-d100-s6     | $2.5 \times 10^2$     | 246            | 8.4                                 | 0.026        | 0.078             |
| m10k-d10-s11     | 49                    | 49             | -                                   | 0.0049       | 0.00              |
| m10k-d10-s12     | 61                    | 61             | -                                   | 0.0061       | 0.00              |
| m10k-d10-s13     | 65                    | 65             | -                                   | 0.0065       | 0.00              |

<sup>&#</sup>x27;s' indicates the random seeds for the turbulence.

 $<sup>^*|</sup>E_{\rm k}|$  and  $|E_{\rm p}|$  are the total kinetic and potential energies of the entire stellar system, respectively. For virialized systems the virial ratio equals 0.5. For models m10k-d10 we did not perform N-body simulations, and therefore their virial ratio is not calculated.

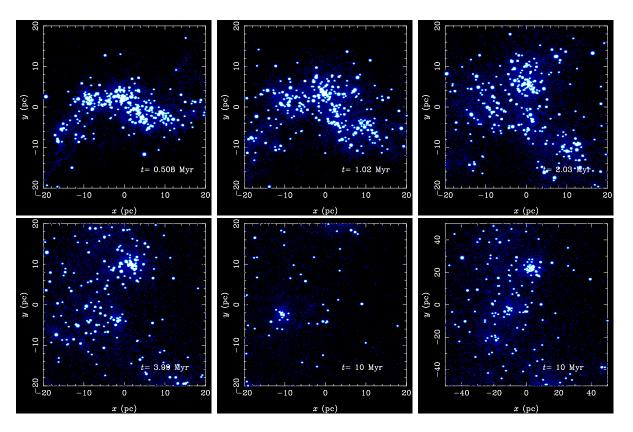


Fig. 2.— Snapshots of model m400k-d100-s3. The size of the dots indicate the masses of the stars:  $8 < m/M_{\odot} < 16$  for the small dots,  $16 < m/M_{\odot} < 40$  for middle sized and  $m > 40 M_{\odot}$  for the largest dots. Stars with a mass  $m < 8 M_{\odot}$  are plotted as small blue dots.

clump mass is  $\sim 100 M_{\odot}$ . Sometimes HOP identifies multiple clumps as one, but by applying the method repeatedly we can separate those again. For this iterative procedure we adopt  $\rho_{\rm out} = \rho_{\rm h,c}$ , where  $\rho_{\rm h,c}$  is the half-mass density of a detected clump. We continue this procedure until  $\rho_{\rm h,c} \gtrsim 100 \rho_{\rm h}$ , after which the clumps are so dense compared to the background that they do not separate anymore in substructures (see Fujii 2015b, for the details).

In Figure 3 we present the mass and half-mass radius of the star clusters obtained from our simulations at t=2 and at  $t=10\,\mathrm{Myr}$ . For comparison, we added a number of observed open clusters (classical open, embedded, young massive, and leaky clusters) to the same diagram. The majority of the identified clusters have masses and radii consistent with those of classical open clusters (Piskunov et al. 2008) (see also Fujii 2015b) and of known embedded clusters (Lada & Lada 2003). The densest initial molecular clouds (m1M-d100, m400k-d100, and m400k-d10) tend to to form massive compact clusters, similar to young massive clusters. Such compact clusters do not form in the less dense or less massive molecular clouds (such as m1M-d1 or m10k-d100).

When observing the 10-Myr-old stellar conglomerates from a distance, they tend to blend in a single star forming region with an average density of  $\sim 0.01 M_{\odot} {\rm pc}^{-3}$ , which is comparable to the mean field density in solar neighborhood (Holmberg & Flynn 2000). Such conglomerates may remain unrecognizable as a cluster system. For those simulations in which no clumps are detected down to a limit of  $100 \, M_{\odot}$ , we adopt the median distance of the stars from the cluster center.

The masses and half-mass radii of the clusters in our simulations mainly resemble the populations of observed embedded and classical open clusters. This result appears to be independent of the initial molecular-cloud density. Embedded and classical open clusters cluster around the point where the cluster age  $(t_{\rm age})$  equals the dynamical time  $(t_{\rm dyn})$  and the half-mass relaxation time  $(t_{\rm rh})$  Fujii (see also 2015b).

Here the dynamical time and the half-mass relaxation time are written as

$$t_{\rm dyn} \sim 2 \times 10^4 \left(\frac{M}{10^6 M_{\odot}}\right)^{-1/2} \left(\frac{r_{\rm h}}{1 {\rm pc}}\right)^{3/2} {\rm year}$$
 (3)

and

$$t_{\rm rh} \sim 2 \times 10^8 \left(\frac{M}{10^6 M_{\odot}}\right)^{1/2} \left(\frac{r_{\rm h}}{1 {\rm pc}}\right)^{3/2} {\rm year},$$
 (4)

respectively (Portegies Zwart et al. 2010), where M is the cluster mass, and  $r_{\rm h}$  is the half-mass radius. For clarity we assumed that the virial radius of star clusters is comparable to the half-mass radius and that the mean stellar mass is  $1\,M_\odot$  (as is the case in our simulations). In Figure 3 we present lines on which the relaxation (black full) and dynamical (black dash-dotted) times are equal to the age of the clusters, respectively. Both lines move as well as all the symbols upward with time.

For the formation of young massive clusters, we find that a dense massive molecular cloud is necessary. The densities required to form such massive clusters exceed the density expected by Larson's relation; the velocity dispersion necessary for the formation of young massive clusters is too high. Such an initial high density may be realized by cloud-cloud collisions (Fukui et al. 2014). The velocity dispersion of our dense model  $\sim 20~\rm km\,s^{-1}$ , which is comparable to the typical relative velocity of molecular clouds associated with young massive clusters such as NGC 3603 and Westerlund 2. For these clusters a collision between two molecular clouds was considered to trigger their formation (Furukawa et al. 2009; Ohama et al. 2010; Fukui et al. 2013, 2014), which is consistent with our findings here.

For forming a star cluster in our simulations, the molecular cloud must be compressive (a high velocity dispersion due to a high density), which is consistent with observations (Zinnecker & Yorke 2007). From various initial conditions, we find that star clusters similar to open, known embedded, and young massive clusters form in these simulations, but leaky clusters ( $M \sim 10^4 M_{\odot}$  and  $r_{\rm h} \sim 10$  pc) must form from different initial conditions. We discuss the formation of leaky clusters in the following section (§ 3.2).

### 3.2. Formation of Leaky Clusters

In the previous section, we show that known embedded, classical open, and young massive clusters form from turbulent molecular clouds, but no leaky cluster is found in our simulations. In this section we address the question: how do leaky clusters form? Is the formation process different from the other clusters?

Pfalzner (2011) proposed that observed embedded clusters grow in mass and size due to star formation and become leaky clusters as a result of the expulsion of the residual gas. This scenario was later explored and the evolutionary tracks of such a cluster on the mass-radius diagram were suggested (Parmentier & Pfalzner 2013; Pfalzner & Kaczmarek 2013; Pfalzner et al. 2014). Portegies Zwart et al. (2010), however, classified the leaky clusters as OB associations. We here do not discuss if the leaky clusters are associations or clusters, but treat both leaky clusters and associations as less dense clustered systems.

We consider leaky clusters (and also OB associations) to form clumpy but that they lose this structure in the early dynamical evolution, contrary to the arguments in Pfalzner (2011). We support our argument with the simulation model m1M-d1-s16 (see the left panels in Figure 4). This simulation started with a spherical molecular cloud that collapsed asymmetrically due to the turbulence velocity field. Stars formed mainly in the densest regions which result in the stellar distribution being elongated and clumpy.

After the residual gas has been removed, the clusters tend to be super virial, and some stars escape right away (see the virial ratio given in Table 2). As a consequence, the entirely stellar distribution expands with time. At an age of  $t=10\,\mathrm{Myr}$  the density of the environment has decreased substantially, and the spatial distribution of the stars resembles leaky clusters and OB associations. In Figure 5 we present the spatial distribution of O and B spectral-type stars in the association Scorpius OB2 (Sco OB2), which can be compared with our simulations in Figure 4.

Sco OB2 is composed of three subgroups; Upper Scorpius (USco), Upper Centaurus-Lupus (Upper Cen-Lup), and Lower Centaurus-Crux (Lower Cen-Crux)

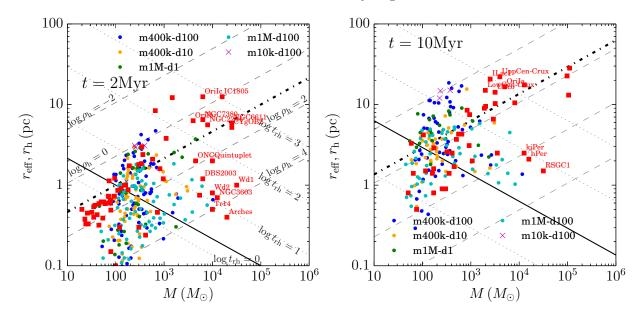


FIG. 3.— Mass-radius diagram of observed and simulated clusters at t=2 and 10 Myr since the start of the N-body simulations. Colored dots are clusters obtained from simulations using a clump finding method. Crosses indicate the median radius and the total mass of the entire stellar system rather than the detected individual clusters. Red squares indicate observed clusters with an age of 1–5 Myr (left) and 5–15 Myr (right). Data are from Piskunov et al. (2008); Winston et al. (2009); Luhman et al. (2003); Andersen et al. (2006); Fang et al. (2009); Levine et al. (2006); Flaherty & Muzerolle (2008); Bonatto & Bica (2011); Horner et al. (1997); Drew et al. (1997); Hodapp & Rayner (1991); Portegies Zwart et al. (2010). Observed clusters with names are the clusters listed in Pfalzner (2009) and Portegies Zwart et al. (2010). Black thick solid and dash-dotted lines indicate the line at which the relaxation time and the dynamical time are equal to the age of the stellar populations. Gray dashed lines indicate the half-mass density of 0.01, 1, 100, and  $10^4 M_{\odot} pc^{-3}$ , and gray dotted lines indicate the half-mass relaxation time of 1000, 100, 10, and 1 Myr from top to bottom. We used the median radius for the observed leaky clusters (Wolff et al. 2007; Pfalzner 2009).

(Wolff et al. 2007). These subgroups are listed in Pfalzner (2009) as leaky clusters, and as associations in Portegies Zwart et al. (2010). They are all located at similar distances from the sun, at 145 pc, 142, and 118 pc, respectively (Wolff et al. 2007), and therefore they are considered to be a system. The distribution of massive (O and B) stars in Sco OB2 is very similar to the distribution of massive stars in model m1M-d1-s16 at an age of 10 Myr.

In figure 6 we present the result of our clump finding analysis for model m1M-d1-s16 at 2 Myr and at 10 Myr. At t=2 Myr we detected  $\sim 20$  clusters that are similar to observed embedded star clusters. At t=10 Myr no clear massive clusters remain visible in the snapshot (see Figure 4), although we still detected several classic open cluster-like structures; in the epoch between 2 Myr to 10 Myr, the stellar distribution has dispersed.

When interpreting the entire system in each simulation as a single association, the mass and radius are very similar to those of observed leaky clusters and OB associations. In figure 6 we present these as crosses (to the top of the panels at 2 Myr and 10 Myr). Model m1M-d1-s16 has a similar appearance and dynamical structure as the Sco OB2 system, rather than the individual sub-clusters USco, Upper Cen-Lups and Lower Cen-Crux. In this analysis we excluded single stars (those with a local density  $\rho_6 < 10^{-3} M_{\odot} {\rm pc}^{-3}$ ) which is more than an order of magnitude lower than the mean density of the solar neighborhood ( $\rho_6$  here is the density measure within the 6 nearest neighbors).

We still detected clumps consistent with open clusters in model m1M-d1-s16. These clumps are the result of the

clumpiness of molecular clouds at a time when we stop the hydrodynamical simulations (at  $\sim 0.9t_{\rm ff,i}$ ). In observed star forming regions, however, stars appear to form when the local density exceeds some threshold density for self-gravitating clouds of  $\sim 10^3 {\rm cm}^{-3}$  (McKee & Ostriker 2007), and feedback starts to dominate the hydrodynamics as soon as the first massive star forms, which may happened well before a free-fall time scale. The free-fall time scale of model m1M-d1-s16 is  $\sim 8 \,\mathrm{Myr}$ , which is considerably longer than the formation time for massive stars  $(\sim 1 \,\mathrm{Myr})$  (McKee & Ostriker 2007). In such a region, where the star forming time scale is considerably smaller than the free-fall time scale of the entire molecular cloud, stellar feedback is expected to terminate the star formation before the molecular cloud fully collapses. This would result in a less clumpy stellar distribution.

Unfortunately in our simulations, we cannot take such gradual star formation and feedback processes into account, although they have been addressed with the AMUSE framework by Pelupessy & Portegies Zwart (2012). In order to mimic the early star formation process, we experimented with stopping the hydrodynamical simulations at an earlier epoch and replace the gas particles with stellar particles.

As in our previous simulations, we assumed that the feedback terminates star formation which causes the residual gas to be ejected instantaneously. We stop the hydrodynamical simulation for model m1M-d1-s16 at  $t=0.65t_{\rm ff,i}$  and  $0.75t_{\rm ff,i}$  (5.3 and 6.2 Myr, respectively), and replace gas particles to stellar particles using the same way as for model m1M-d1-s16, i.e., assuming a local star

formation efficiency given by equation (2) and the same values for  $\alpha_{\rm sfe}=0.02$ . The numbers of stars that form using this procedure decrease considerably, and the resulting virial ratio of the stellar system increases. We also run the same initial conditions but with different random seeds (m1M-d1-s15 and m1M-d1-s17). In Table 2 we present some global parameters for these models.

Snapshots of these models (m1M-d1-s16-t0.75 and m1M-d1-s16-t0.65) are shown in the middle and right panels of Figure 4. The distribution of massive stars is less clumpy compared with that of model m1M-d1-s16 (standard model, in which the hydrodynamical simulation is stopped at  $0.9t_{\rm ff}$ ; see the left panels of Figure 4). We also apply the clump finding algorithm to these models, and the results of which are shown in Figure 6. At t = 2Myr, several clumps are detected in both models, but they are less dense compared with those detected in our standard model. In model m1M-d1-s16-t0.65 in particular, the density of the detected clumps is only slightly elevated compared to the background density in the solar neighborhood  $(0.01 M_{\odot} \text{pc}^{-3})$  (Holmberg & Flynn 2000), and these clumps may therefore not be recognized as clusters. In model m1M-d1-s16-t0.75 some clumps which resemble open clusters are still detected at t = 10 Myr, but none in model m1M-d1-s16-t0.65. If we treat the entire system as a one cluster, the masses are similar to those of leaky clusters and associations, even though the size remains larger by about a factor of two. On Figure 6 we present the resulting clusters with a mass and half-mass radius in stars with  $\rho_6 > 10^{-3} M_{\odot} \text{pc}^{-3}$ .

Our assumption that star formation terminates instantaneously throughout the system after about one freefall time of the molecular cloud probably overestimates the effect of the feedback considerably. In observed star-forming regions the feedback from massive stars tend to limit star formation locally, but may not affect the entire ( $\sim 100~\rm pc$  across) star forming region. In the simulations of Pelupessy & Portegies Zwart (2012), the wind of one massive  $\sim 30 M_{\odot}$  star blows the residual gas from the clustered environment in a couple of Myr, which is much longer than adopted in our simulations.

If star formation proceeds as clumpy as simulated here, the feedback is even more localized, which will result in a considerable age spread among subgroups. Our simulations would then be representative for the formation of cluster complexes such as USco, Upper Cen-Lups, and Lower Cen-Crux, or OB association such as Sco OB2. The ages of these three subgroups are slightly different each other; 14–15, 11–12, and 5–6 Myr for Upper Cen-Lup, Lower Cen-Crux, and USco, respectively (Wolff et al. 2007). If we could assume local feedback processes, an association (or leaky clusters) similar to Sco OB2 might form from an initial condition such as models m1M-d1. Less dense clusters tend to have a wider age spreads (Parmentier et al. 2014), which is also consistent with our simulations. We therefore argue that the ancestors of associations are conglomerates of denser embedded clusters. We detect these as an environment with multiple low-mass but rather dense clusters that disperse in time. The evaporation of these clusters is driven by relaxation and feedback, and this makes them resemble associations.

#### 4. INITIAL CONDITIONS OF MOLECULAR CLOUDS

In the previous section, we showed that our dense models tend to form young massive clusters and that less dense models lead to leaky clusters as well as known embedded and classic open clusters. The types of the resulting star cluster is sensitive to the initial conditions of the parental molecular clouds. In this section, we compare our initial conditions with observed molecular clouds and discuss a model for the formation of clusters in the Milky Way and other nearby galaxies.

In Figure 7, we present the mass and density of individual molecular clouds observed in the Milky Way and those estimated for local disk and starburst galaxies (Krumholz et al. 2012). We also show the initial conditions of our simulations. The dashed line in the Figure 7 indicates the Larson's relation. In order to estimate the mass of molecular clouds following Larson's law, we assume that the molecular clouds are in virial equilibrium (i.e., they satisfy  $\sigma_{\rm g}^2 = GM_{\rm g}/r_{\rm g}$ , where  $\sigma_{\rm g}$ ,  $M_{\rm g}$ , and  $r_{\rm g}$  are the velocity dispersion, mass, and radius of the molecular clouds, respectively). Observed molecular clouds, however, are not necessarily virialized.

Molecular clouds in the Milky Way tend to follow Larson's relation, but with a large scatter of the density. On the other hand, not all of our initial conditions are consistent with the mass and density of molecular clouds observed in the Milky Way. Models m10k-d100 ( $10^4 M_{\odot}$  and  $100 M_{\odot} \text{pc}^{-3} \simeq 1700 \text{cm}^{-3}$ ) and m10k-d10 ( $10^4 M_{\odot}$  and  $10 M_{\odot} \text{pc}^{-3} \simeq 170 \text{cm}^{-3}$ ), for example, are initially indistinguishable from typical molecular clouds in the Milky Way.

As we described in section 3, the number of stars formed in model m10k-d10 was too small (fewer than 100 stars) to be recognized as a cluster in our analysis. Model m10k-d100 produces a sufficiently large number of stars but does not form a recognizable cluster after 2 Myr. If we treat the entire region of this model as a cluster conglomerate, the mass and radius is similar to that of an open cluster. From this, we conclude that the molecular clouds typical in the Milky Way tend to form classical open clusters, but that they are insufficiently massive and dense to form massive star clusters.

Model m1M-d1 ( $10^6 M_{\odot}$  and  $1 M_{\odot} \mathrm{pc}^{-3}$ ) represents the most massive molecular cloud in the Milky Way (Murray 2011), and it follows Larson's relation. This initial condition results in several embedded cluster cores, that eventually evolve to a conglomerate of associations.

The initial conditions which tend to form young massive clusters are considerably denser than the molecular clouds observed in the Milky Way (see Figure 7). To form a young massive clusters in our simulations a mass of at least several  $10^5 M_{\odot}$  and a mean density of  $10 M_{\odot} {\rm pc}^{-3}$  (170 cm<sup>-3</sup>) is required. Such initial conditions are common in local starburst galaxies, but very rare in the Milky Way.

In Figure 7 we present the estimated mass and molecular clouds density typical for local starburst and disk galaxies. This data is obtained from Krumholz et al. (2012). We calculated the masses and densities for these molecular clouds from the free-fall time scale provided by Krumholz et al. (2012) using the observed surface gas densities ( $\Sigma_g$ ). In Krumholz et al. (2012) they considered two rather distinct regimes of molecular clouds; these are the molecular cloud regime and the Toomre regime. The

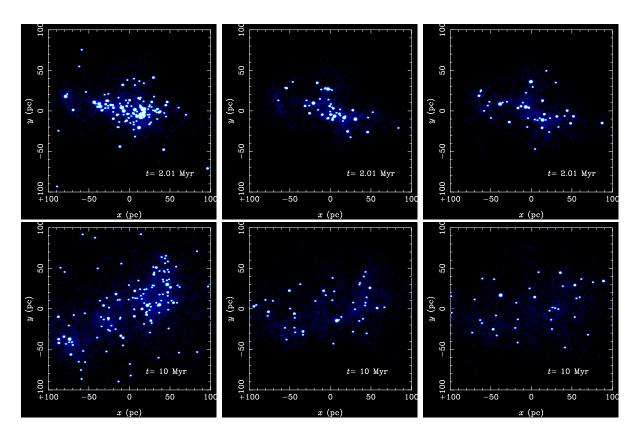


Fig. 4.— Snapshots at t=2 (top) and 10 (bottom) Myr for model d1-1M, but for different timing of gas removal. t=0.9, 0.75, and  $0.65t_{\rm ff,i}$  (models m1M-d1-s16, m1M-d1-s16-t0.75, and m1M-d1-s16-t0.65) from left to right.

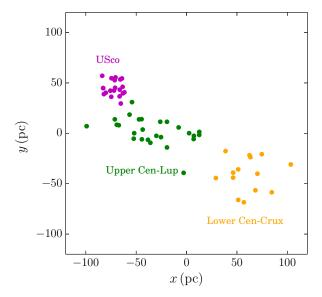


Fig. 5.— Positions of B-type stars which belong to USco (magenta), Upper Cen-Lup (green), and Lower Cen-Crux (orange). Data is from Wolff et al. (2007). We assume 140 pc as the distance (Wolff et al. 2007).

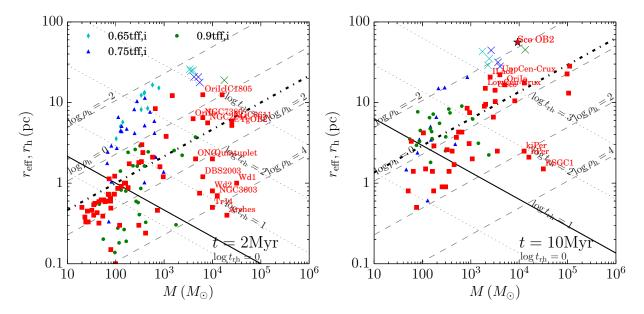


Fig. 6.— Mass-radius diagram of detected clusters for models m1M-d1-s16 (green dots), m1M-d1-s16-t0.75 (blue triangles), and m1M-d1s16-t0.65 (cyan diamonds) at t=2 and 10 Myr. Red squares indicate observed young clusters; clusters with an age of 1–5 Myr and 5–15 Myr are plotted in top and bottom panels, respectively. The data for the observed clusters are the same as those in Figure 3. The mass and half-mass radii of simulations, interpreted as unresolved clusters, are shown as crosses; each cross represents a single simulation.

molecular cloud regime is expected to be common in local disk galaxies. The molecular clouds are decoupled from their surrounding interstellar medium, and as a result self-gravitating (Krumholz et al. 2012). The Toomre regime is common in starburst galaxies. In this case the interstellar medium is highly turbulent and therefore the free-fall time scale of the molecular clouds should be estimated using the mid-plane pressure in the galactic disks (see Krumholz et al. 2012, for the details).

Following the description of Krumholz et al. (2012), we estimate the typical mass of molecular clouds for each galaxy listed in Krumholz et al. (2012). We take the smaller free-fall time scale for the molecular cloud and Toomre regimes ( $t_{\rm ff,GMC}$  and  $t_{\rm ff,T}$ , respectively) as the free-fall time scale  $(t_{\rm ff})$ , which is consistent with Krumholz et al. (2012). We calculate the density through the free-fall time scale using:

$$\rho_{\rm g} = \frac{3\pi}{32Gt_{\rm ff}^2}.\tag{5}$$

In the Toomre regime, the mid-plane pressure in the disk of surface gas density  $\Sigma_{\rm g}$  is

$$P = \rho_{\rm g,T} \sigma_{\rm g}^2 = \phi_P \frac{\pi}{2} G \Sigma_{\rm g}^2.$$
 (6)

Here  $\rho_{g,T}$  is the molecular cloud density in the Toomre regime,  $\sigma_g$  is the velocity dispersion of the gas and  $\phi_P$  is a dimensionless factor (Krumholz et al. 2012). The Toomre Q for the gas is written as

$$Q = \frac{\sqrt{2(\beta+1)}\sigma_{\rm g}\Omega}{\pi G \Sigma_{\rm g}}.$$
 (7)

Here  $\beta$  is the logarithmic index of the rotation curve  $(\beta = 0 \text{ for a flat rotation curve, whereas for solid-body})$ rotation  $\beta = 1$ ),  $\Omega = 2\pi/t_{\rm orb}$  ( $t_{\rm orb}$  is the galactic orbital period) is the angular velocity of galactic rotation (see also Krumholz & McKee 2005). From these equations, the density of the molecular cloud becomes

$$\rho_{\rm g,T} \simeq \frac{(\beta+1)\phi_P \Omega^2}{\pi G Q^2}.$$
(8)

Here we adopt  $Q \sim 1$  and  $\beta = 0$  following Krumholz et al. (2012). If we assume that the cloud is virialized — i.e.,  $\sigma_{\rm g}^2 \sim G M_{\rm g,T}/r_{\rm g}$ , where  $M_{\rm g,T}$  and  $r_{\rm g}$  are the mass and radius of the cloud— from equation (7) and  $\rho_{\rm g,T} = 3 M_{\rm g,T}/(4\pi r_{\rm g}^3)$  we can estimate the cloud mass using:

$$M_{\rm g,T} \sim \frac{1}{32} \sqrt{\frac{3}{\pi}} G^{3/2} \Sigma_{\rm g}^3 t_{\rm orb}^3 \rho_{\rm g}^{-1/2}.$$
 (9)

 $M_{\rm g,T} \sim \frac{1}{32} \sqrt{\frac{3}{\pi}} G^{3/2} \Sigma_{\rm g}^3 t_{\rm orb}^3 \rho_{\rm g}^{-1/2}. \tag{9}$  Because for each galaxy  $t_{\rm orb}$  and  $\Sigma_{\rm g}$  are given in Krumholz et al. (2012), we can estimate the cloud density and mass from equation (8) and (9). Here we adopt  $\phi_P \simeq 3$ , following Krumholz et al. (2012).

For the molecular cloud regime (i.e.,  $t_{\rm ff,GMC} < t_{\rm ff,T}$ ), the mass is estimated as follows. The mass of molecular clouds is estimated by the two-dimensional Jeans mass in galactic disks (Kim & Ostriker 2002; McKee & Ostriker 2007;

Chandar et al. 2011), which is given by 
$$M_{\rm g,GMC} = \frac{\sigma_{\rm g}^4}{G^2 \Sigma_{\rm g}}, \tag{10}$$

(see equation (3) of Krumholz et al. 2012). Since the mass and density of molecular clouds in the molecular cloud regime are written as  $M_{\rm g,GMC}=\pi r_{\rm g}^2 \Sigma_{\rm GMC}$  and  $\rho_{\rm g,GMC}=$  $(3/4\pi)M_{\rm g,GMC}r_{\rm g}^{-3}$ , where  $\Sigma_{\rm GMC}$  is the surface density of molecular clouds, and using equation (10) we can calculate the density of molecular clouds with (equation (4) in Krumholz et al. 2012):

$$\rho_{\rm g,GMC} = \frac{3\sqrt{\pi}}{4} \frac{G\sqrt{\Sigma_{\rm GMC}^3 \Sigma_{\rm g}}}{\sigma_{\sigma}^2}.$$
 (11)

Here we adopt  $\Sigma_{\rm GMC}=85M_{\odot}{\rm pc}^{-2}$  and  $\sigma_{\rm g}=8~{\rm km\,s^{-1}}$  for all galaxies following Krumholz et al. (2012). From equations (10) and (11), we obtain the mass and density in the molecular cloud regime using the value for  $\Sigma_{\rm g}$  from Krumholz et al. (2012).

The obtained masses and densities for molecular clouds in the local disk and starburst galaxies are presented in Figure 7. Most galaxies are in the Toomre regime (and only 13 disk galaxies are in the molecular cloud regime). The molecular clouds typical for starburst galaxies are factors of 10 to 100 denser than those following Larson's relation. Our massive and dense models (m400k-d100, m400k-d10, and m1M-d100), which form young massive clusters, are consistent with the molecular cloud observed in starburst galaxies. Starburst galaxies such as M83 (Bastian et al. 2011) and M51 (Chandar et al. 2011) are indeed rich in dense massive clusters. On the other hand, molecular clouds typical in local disk galaxies do follow Larson's relation. Our model m1M-d1, which forms classical open and leaky clusters (associations), appears to be quite similar to these molecular clouds.

The typical molecular cloud in a disk galaxy, such as the Milky Way, tends to form classical open clusters and associations, but these clouds are insufficiently massive to form young massive star clusters. This is consistent with the abundance of open star cluster and associations in the Milky Way and with the lack of massive star clusters. According to our simulations, the formation of a massive star cluster requires a massive ( $\sim 10^5$ – $10^6 M_{\odot}$ ) and dense  $(\sim 10-100 M_{\odot} \text{pc}^{-3})$  molecular cloud. Such a massive molecular cloud has, if virialized, a velocity dispersion of  $\sim 20 \rm km \, s^{-1}$ . Such a high velocity dispersion (under compressive condition) could result from the collision between two clouds (Furukawa et al. 2009; Ohama et al. 2010; Fukui et al. 2014). Comparable high velocities are observed in the regions surrounding young massive clusters, such as in the vicinity of NGC 3603 (Fukui et al. 2014) and Westerlund 2 (Furukawa et al. 2009; Ohama et al. 2010). These clusters are claimed to have been the result of cloudcloud collisions (Furukawa et al. 2009; Ohama et al. 2010; Fukui et al. 2014). These claims are supported by threedimensional magneto-hydrodynamics simulations, which also suggest that such cloud-cloud collisions initiate the formation of massive cloud cores and potentially form massive star clusters (Inoue & Fukui 2013).

Although our initial conditions of molecular clouds cover a relatively wide range of mass and density, they are limited in our choice of opting for homogeneous-density spheres. Recent numerical studies indicate that molecular clouds with a concentrated density profile such as a power-law, tend to form one high-mass star in the center surrounded by many low-mass stars (Girichidis et al. 2011, 2012). Such centrally concentrated models then may more efficiently lead to the formation of massive clusters than our adopted homogeneous initial conditions.

# 5. THE MASS AND RADIUS EVOLUTION OF YOUNG STAR CLUSTERS

Star clusters can be subdivided in several types, which represent themselves clearly when presented in a massradius diagrams. The mass-radius distribution of star clusters changes with time. Here we discuss the time evolution of the mass and radius of young clusters.

#### 5.1. Observations

We start with summarizing the mass and radius evolution of observed young star clusters. These observations are presented in Figure 8, in particular for observed embedded clusters, classical open star clusters, young massive (starburst) clusters and associations (Lada & Lada 2003; Piskunov et al. 2008; Winston et al. 2009; Luhman et al. 2003; Andersen et al. 2006; Fang et al. 2009; Levine et al. 2006; Flaherty & Muzerolle 2008; Bonatto & Bica 2011; Horner et al. 1997; Drew et al. 1997; Hodapp & Rayner 1991; Pfalzner 2009; Portegies Zwart et al. 2010). For clarity we bin the clusters in age in intervals of  $t_{\rm age} = 1-5\,{\rm Myr},\,5-20\,{\rm Myr},\,{\rm and}\,20-100\,{\rm Myr}.$ 

Pfalzner (2009) and Portegies Zwart et al. (2010) list several young massive clusters, but in many cases the listed radii differ. We adopt the half-mass radius given in Portegies Zwart et al. (2010), because the radius presented in Pfalzner (2009) correspond to the core radius of the clusters rather than the half-mass radius. The former gives a more direct comparison with our simulations. In our analysis we try to stay as much as possible to the same definition of cluster radius. Piskunov et al. (2008) present projected core and tidal radii by fitting King models (King 1966). Because the density profiles for the open clusters listed in Piskunov et al. (2008) are very shallow, we adopted their core radii, which for a King model with  $W_0 = 3$  is quite similar to the half-mass radius (the ratio of the three-dimensional core radius to half-mass radius is 0.65 for a King model with  $W_0 = 3$ ).

Embedded clusters observed in the Milky Way galaxy reside almost exclusively in the left panel of the mass-radius diagram (t = 1-5 Myr panel in Figure 8) because they are young by definition. Embedded and classical open clusters populate the same region (at the bottom left in the same panel). These clusters tend to grow in size with age, which is a consequence of relaxation and out gassing; embedded clusters observed in the Milky Way therefore appear as ancestors of classical open clusters (Fujii 2015b). Associations populate the top right region of the left and middle panels ( $t = 1-5 \,\mathrm{Myr}$  and  $5-20 \,\mathrm{Myr}$ , respectively), and young massive clusters are found to the right in the diagrams in Figure 8. As was already suggested by Pfalzner (2009), young massive star clusters are well separated in mass and radius from embedded and open clusters. This separation, however, diminishes for the older age group (20–100 Myr, see the right panel of Figure 8).

## 5.2. Analytic model for the dynamical evolution of young star clusters

The distribution and evolution of the observed star clusters in mass and radius can be understood from out models of the dynamical evolution for star clusters.

The lower limit of the cluster density can be understood by considering the background density in the field. The magenta dashed line in the diagram indicate  $\rho = 0.1 M_{\odot} {\rm pc}^{-3}$ , which is an order of magnitude higher than the mean density of the field stars in the solar neighborhood (Holmberg & Flynn 2000). We adopt  $\rho = 0.1 M_{\odot} {\rm pc}^{-3}$  as a lower limit for the cluster density (magenta dashed line in Figure 8). Star clusters with a density similar to or lower than the mean stellar density would therefore not be recognizable as clusters. And indeed, only a few of the most massive clusters reside above

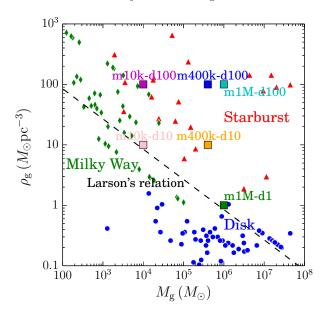


Fig. 7.— Mass-density relation of observed molecular clouds. Green diamonds indicate individual molecular clouds in the Milky Way galaxy. Blue circles and red triangles are for molecular clouds typical in individual local disk and starburst galaxies, respectively. Each point indicates one galaxy. The data is from Krumholz et al. (2012). Color squares indicate our initial conditions which are the same as those shown in Figure 1. Dashed line indicates the mass-density relation following Larson's law for virialized cloud ( $\sigma_g^2 = GM_g/R_g$ ).

this curve, and those have a relatively high concentration. As a consequence, their core densities exceed the local density considerably, which helps to identify them as clusters in observational campaigns.

The blue dash-dotted lines in Figure 8 indicate the massradius relation for which the dynamical time scale (see equation (3)) is equal to the age of the cluster. Each panel contains two lines, one for the minimum and one for the maximum age of the clusters shown in the pan-The regions between these lines is shaded blue. Clusters between or below the blue lines will be recognizable as a bound systems unless the lines exceed the magenta dashed line. Portegies Zwart et al. (2010) and Gieles & Portegies Zwart (2011) argued that the ratio between cluster age and the dynamical time provides a good indicator for separating the bound from the unbound systems: They adopt as a criterion  $t_{\rm age}/t_{\rm dyn} \gtrsim 3$  to make this distinction. Using this criterion they categorized the leaky clusters in Pfalzner (2009) as associations. The blue region in Figure 8 moves upward with time, together with the observed clusters. At t > 20 Myr (the right panel in Figure 8) the blue lines are located above the magenta line, indicating that these clusters have a density too low to be recognized as a cluster.

The evolution of dense star clusters is quite different from those of open clusters or associations. Dense star cluster evolution can roughly be divided in two phases; before core collapse and after core collapse. In the former phase the core radius of the star clusters shrinks, and as a consequence, its core density increases (Hénon 1965; Lynden-Bell & Wood 1968). From the moment the first hard binaries form in the cluster core (Spitzer & Hart 1971; Aarseth 1974), they act as an energy sources (Heggie 1975; Hut 1983) causing the core to re-expand. From this moment on, the core- and half-mass radius of clusters in-

creases. These processes proceed on the half-mass relaxation time:

$$t_{\rm rh} = \frac{0.065\sigma^3}{G^2 \langle m \rangle \rho \ln \Lambda}.$$
 (12)

Here  $\sigma$  and  $\rho$  are the velocity dispersion and density of the cluster, respectively, and  $\ln \Lambda$  is the Coulomb logarithm (Spitzer 1987). We rewrite equation (12) to include some common dimensions in equation (4).

Gieles et al. (2011) modeled the post-collapse evolution of the half-mass radius and the density of star clusters due to the energy flux from the core following the description of Hénon (1965). We attempt to understand the dynamical evolution of young star clusters using their description. We ignore the pre-collapse phase and consider only the evolution in the post-collapse (expansion) phase, because the pre-collapse phase is much shorter than post-collapse. The core-collapse time, which is the time for the pre-collapse phase, scales with the relaxation time (see equation (4) or (12)). This time scale depends on the stellar mass function, and for clusters with a realistic mass function the core collapse time is generally shorter than one relaxation (Portegies Zwart & McMillan 2002; Gürkan et al. 2004; Fujii & Portegies Zwart 2014). Since most of young open clusters in our observed sample have a relaxation time  $\lesssim 10 \,\mathrm{Myr}$  (see the left panel of Figure 8), they probably reach core collapse well within a few Myr. We also ignore the effect of the Galactic tidal field, because the time scale we treat here is short (< 100 Myr) compared to the time scale for the tidal disruption ( $\sim 1 \, \text{Gyr}$ ) (Gieles et al. 2007).

The time of the half-mass radius of clusters due to binary heating in the core is given by equation (B7) in Gieles et al. (2011):

$$r_{\rm h} \simeq \left(\frac{3G}{4\pi N}\right)^{1/3} (125\zeta t)^{2/3}.$$
 (13)

Here N is the initial number of stars in the cluster. In equation (B7) in Gieles et al. (2011), the cluster mass is assumed that  $M=\langle m\rangle N$ , where  $\langle m\rangle$  is the mean stellar mass. They adopted a scaled mass  $\langle m\rangle=0.5$  and as a result their equation (B7) is slightly different from our equation. If we assume that  $\langle m\rangle=0.5\,M_{\odot}$ , we can write this equation as

$$r_{\rm h} \simeq 2.0 \, \zeta^{2/3} \left(\frac{M}{M_{\odot}}\right)^{-1/3} \left(\frac{t_{\rm age}}{\rm Myr}\right)^{2/3} \, {\rm pc}.$$
 (14)

Here we adopt  $t=t_{\rm age}$  because we ignore the pre-collapse phase. The the expansion-rate coefficient,  $\zeta$ , depends on the ratio of the maximum to the minimum mass in the stellar mass function,  $\mu \equiv m_{\rm max}/m_{\rm min}$ . In Gieles et al. (2011) we use  $\zeta \simeq 0.2$ , which corresponds to  $\mu \simeq 10$ , and which is appropriate for globular clusters. Young clusters however, should have a larger value of  $\mu$  because of the presence of massive stars. For some of these clusters  $m_{\rm max}/m_{\rm min} \simeq 100\,M_{\odot}/0.01\,M_{\odot} \simeq 10^4$ . Following Gieles et al. (2011) and assuming  $\zeta \propto \mu^{1/2}$ , we obtain  $\zeta \simeq 20$  for  $\mu \simeq 10^4$ . Equation (14) with  $\zeta = 20$  for  $t = t_{\rm age} = 2$ , 10, 40 Myr is shown as green dashed lines in Figure 8.

The majority of the observed clusters are located below this evolutionary line rather than straddling the line, which indicates that they have  $\zeta < 20$ . Green dotted lines in each panel of Figure 8 shows equation (14) with  $\zeta = 0.2$ . Most of observed embedded and classical open clusters are located between the dotted green (for  $\zeta = 0.2$ ) and the dashed green ( $\zeta = 20$ ) lines. This may be caused by the large dispersion in  $\zeta$ , as we discussed here, or because the pre-collapse time is not taken into account in our analysis. By ignoring the pre-collapse time we reduce the evolution time of a star cluster compared to the expectation.

The descriptions of Gieles et al. (2011) (equations (13) and (14)) give infinite density at t = 0 Myr, which hardly seems realistic for actual young star clusters. Instead, we adopt equation (B4) of Gieles et al. (2011):

$$\rho_{\rm h} \simeq \frac{1}{G} \left( \frac{N}{250\zeta t} \right)^2, \tag{15}$$

which gives the half-mass density as a function of time. We also adopt  $\langle m \rangle = 0.5\,M_{\odot}$ . We assume a (maximum) half-mass density of  $10^4M_{\odot}{\rm pc}^{-3}$  at  $t_{\rm age}=0.1$  Myr irrespective of the cluster mass; we obtain  $\rho_{\rm h}(M_{\odot}{\rm pc}^{-3})=100(t/{\rm Myr})^{-2}$ . Since  $\rho_{\rm h}=3M/(8\pi r_{\rm h}^3)$ , the relation can be written as

$$r_{\rm h} = 0.0158 \left(\frac{M}{M_{\odot}}\right)^{1/3} \left(\frac{t_{\rm age}}{\rm Myr}\right)^{2/3} (\rm pc).$$
 (16)

Equation (16) is presented in Figure 8 as the solid green line. One naively expects that clusters with an initial density smaller than  $10^4 M_{\odot} {\rm pc}^{-3}$  populate the area above this line, which is consistent with the observations. From a theoretical perspective we argue that star clusters are expected to reside in the green and blue regions in Figure 8, which for the majority of observed clusters appear to be the case.

From these results, the regions in which clusters are expected to exist on mass-radius diagrams are shown by green and blue shades in Figure 8, and observed distribution of star clusters matches them. Furthermore, our

analytic models suggest two distinct populations of massive ( $\sim 10^4 M_{\odot}$ ) clusters, which are called as starburst and leaky clusters by Pfalzner (2009). We argue that these two populations naturally appear if we consider the formation and the dynamical evolution process of star clusters.

# 5.3. Time evolution of cluster radius: Leaky and starburst clusters

Young star clusters with  $M \sim 10^4 M_{\odot}$  are divided into two groups, as can be seen in Figure 8. Pfalzner (2009) named them starburst (young massive) clusters and leaky clusters (following Portegies Zwart et al. (2010) we identify the latter category as associations). Pfalzner (2009) and Pfalzner (2011) showed that both families of clusters expand with time, but at a different rate:  $r/\text{pc} = 0.16(t_{\text{age}}/\text{Myr})$  for the starburst clusters and  $r/\text{pc} = 3.5(t_{\text{age}}/\text{Myr})^{2/3}$  for the associations. In this section, we discuss the origin of these different evolutionary tracks.

In Figure 9 we present the age and radius of observed in young star clusters with a mass of  $10^3 < M < 10^5 M_{\odot}$ . The time evolution for cluster radii, plotted as the solid green lines, are obtained from the analytic models discussed in § 5.2.

Associations are about one dynamical time scale old, and therefore we can hardly confirm weather they are bound or not. If we consider them to be one dynamical timescale old, i.e.,  $t_{\rm age} \simeq t_{\rm dyn}$ , equation (3) gives  $r_{\rm h}/{\rm pc} = 2.7(t_{\rm age}/{\rm pc})^{2/3}$ . We present this relation in Figure 9 as the top green line. The model is consistent with the observed clusters, and the power-law index of our model is consistent with that of Pfalzner (2011).

For starburst clusters, we adopt the results based on Gieles et al. (2011). By adopting  $M=10^4 M_{\odot}$  in equation (16), we obtain  $r_{\rm h}/{\rm pc}=0.34(t_{\rm age}/{\rm Myr})^{2/3}$ . We present this relation in Figure 9 as the bottom green line. In part due to the large scatter, this relation is also consistent with the observed radius evolution of starburst clusters.

The magenta dash-dotted line in Figure 9 gives the relation  $\rho_{\rm h} = 0.1 M_{\odot} {\rm pc}^{-3}$ . This is an order of magnitude higher than the field density at solar neighborhood  $(0.01 M_{\odot} {\rm pc}^{-3})$  (Holmberg & Flynn 2000) and we assume this to be a minimum to the (observable) cluster density. This predict that associations will not survive more than  $\sim 20$  Myr, and indeed no such a cluster has been observed.

#### 6. SUMMARY

We performed a series of simulations of star forming regions. Our calculations start with hydrodynamical simulations of turbulent molecular clouds. These simulations are continued for about one initial free-fall time scale, after which we replace gas particles with stars adopting a local star formation efficiency (Krumholz et al. 2012). The stellar mass are selected randomly from the adopted initial mass function, and the stars receive the position and velocity of the gas particles they replace. We subsequently removed all residual gas and continue the evolution of the young emerging star cluster by means of N-body simulations with stellar evolution.

The types of star clusters that formed in our simulations depend on the initial conditions (mass and density) of the molecular cloud. The clouds with initial conditions typical

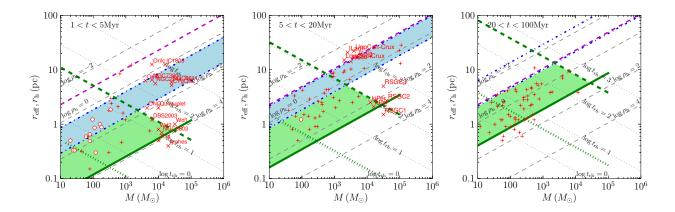


Fig. 8.— Mass-radius diagrams of observed young star clusters for  $t_{\rm age}=1-5$ , 5–20, and 20–100 Myr from left to right. The data is from Lada & Lada (2003) for embedded clusters (red circles), Piskunov et al. (2008); Winston et al. (2009); Luhman et al. (2003); Andersen et al. (2006); Fang et al. (2009); Levine et al. (2006); Flaherty & Muzerolle (2008); Bonatto & Bica (2011); Horner et al. (1997); Drew et al. (1997); Hodapp & Rayner (1991) for open clusters (red pluses), and Portegies Zwart et al. (2010) for young massive clusters and leaky clusters (red crosses). The data for the leaky clusters are overlapped with Pfalzner (2009). The clusters listed in Portegies Zwart et al. (2010) are shown with the names.

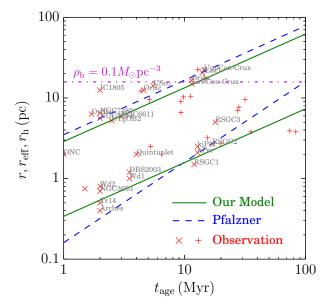


FIG. 9.— Cluster radius as a function of time for clusters with a mass of  $10^3-10^5 M_{\odot}$ . Red plus-signs are from Portegies Zwart et al. (2010) and red pluses from the others (see the caption of Figure 8). Blue dashed lines are the relation given in Pfalzner (2011) and Pfalzner (2009):  $r = 3.5 t_{\rm age}^{2/3}$  and  $r = 0.16 t_{\rm age}$  for top and bottom, respectively. Green lines are cluster radii as a function of time obtained from our model:  $r_{\rm h} = 2.7 t_{\rm age}^{2/3}$  and  $r_{\rm h} = 0.34 t_{\rm age}^{2/3}$  for top and bottom, respectively. Note that for starburst clusters, we plot the half-mass radii given in Portegies Zwart et al. (2010) instead of "size" in Pfalzner (2009).

for those observed in the Milky Way  $(10^4 M_{\odot} \text{ and } 100\text{--}1000 \text{ cm}^{-3})$  lead to classical open clusters. More massive clouds  $(10^5\text{--}10^6 M_{\odot})$  with the same density evolve into dense massive clusters. These massive molecular clouds are common in starburst galaxies, but are very rare in local disk galaxies such as the Milky Way. This result is consistent with observations that young massive clusters are common in starburst galaxies, but only several has been found in the Milky Way. We argue that such massive clouds must be able to form in the Milky Way Galaxy, even though they are probably rare.

Dense massive clusters in our simulation form from molecular clouds with a mass of  $10^6 M_{\odot}$  and a density of  $\sim 1000~\rm cm^{-3}~(100 M_{\odot} \rm pc^{-3})$  leading to a velocity dispersion of  $\sim 20~\rm km\,s^{-1}$ . This is consistent with the relative velocity of molecular clouds observed near young massive clusters in the Milky Way such as near NGC 3603 (Fukui et al. 2014) and Westerlund 2 (Furukawa et al. 2009; Ohama et al. 2010). We argue that massive clusters in the Milky Way can therefore not form from individual clouds, but their formation may have been initiated in cloud-cloud collisions (Furukawa et al. 2009; Ohama et al. 2010; Fukui et al. 2014).

Molecular clouds with a mass of  $\sim 10^6 M_{\odot}$  and a low density of  $\sim 10 \, \rm cm^{-3}$  ( $\sim 1 M_{\odot} \rm pc^{-3}$ ), which follow Larson's relation, tend to form associations ("leaky clusters" in the terminology of Pfalzner (2009)). These relatively low density and massive molecular clouds form a number of small clumps. They might be detected as embedded or classical open clusters when they are young, but they evolve to less dense clusters due to the gas expulsion and relaxation. After several Myr, these systems lose their clumpiness and become recognizable as associations.

In our simulations we assumed that stars form instantaneously upon the expulsion of the residual gas (after an initial free-fall time of the molecular cloud). Our prescription for star formation is simple compared to reality, in which star formation triggers the expulsion of the residual gas by means of feedback processes. Regardless the simplicity of our approach, we are still able to make a distinction between the formation of associations, open clusters, and massive star clusters.

The young stellar system, Sco OB2, is an assembly of associations of slightly different ages, USco, Upper Cen-Lups, and Lower Cen-Crux. A stellar system similar to Sco OB2 naturally originates in our simulations of relatively massive and low-density molecular clouds, although the age spread cannot be reproduced with our method. The relation that less dense clusters have wider age spreads of stars is observationally and theoretically suggested (Parmentier et al. 2014).

In addition, we compared our simulations with theo-

retical models for cluster expansion due to the dynamical evolution (Gieles et al. 2011). These models satisfactorily explain the evolution in radius of simulated clusters as well as the observed clusters.

We also found that the distribution of clusters on the mass-radius diagram is also limited by the density with which the dynamical time scale is equal to the cluster age. This implies that if the cluster age is much shorter than the dynamical time; such clusters cannot be recognized as (bound) systems (Gieles & Portegies Zwart 2011). After  $\simeq 20$  Myr the density of these associations drops below the background density and dissolve.

The gap of the radius distribution for associations and young massive clusters suggested by Pfalzner (2009) is consistent with our simulation results. While young massive clusters evolve following the cluster expansion model, leaky clusters have  $t_{\rm age} \sim t_{\rm dyn}$ . With our models, the evolution of radius for observed leaky and young massive clusters are described by  $r_{\rm h}/{\rm pc} = 2.7 (t_{\rm age}/{\rm pc})^{2/3}$ and  $r_h/pc = 0.34(t_{age}/Myr)^{2/3}$ , respectively. These are also consistent with observations. Pfalzner et al. (2014) claimed that star formation continues in embedded clusters and that after the gas expulsion they expand and become associations. Our models however indicate that clumpy star forming regions are observed as a conglomerate of embedded clusters, but at a later time these systems lose their clumpiness due to the expulsion of the residual gas and two-body relaxation. Because our coverage of parameter space remains limited and much is still to be uncovered, we hope to explore a much wider range of initial conditions of molecular clouds (different masses, radii, and density distributions) and other assumption for star formation (different epochs for star formation and gradual gas removal rather than instantaneous gas expulsion).

Our results suggest that the difference in the parental molecular clouds results in the formation of various types of star clusters if we assume the same star formation process and that the cluster formation process does not depend on the condition of the galaxy, either normal disk or starburst.

We thank the anonymous referee for useful comments. This work was supported by JSPS KAKENHI Grant Number 26800108 and NAOJ Fellowship, the Netherlands Research Council NWO (grants #643.200.503, #639.073.803 and #614.061.608), and the Netherlands Research School for Astronomy (NOVA). Numerical computations were partially carried out on Cray XC30 at the Center for Computational Astrophysics (CfCA) of the National Astronomical Observatory of Japan and Little Green Machine at Leiden Observatory.

### REFERENCES

Aarseth, S. J. 1974, A&A, 35, 237
Andersen, M., Meyer, M. R., Oppenheimer, B., Dougados, C., & Carpenter, J. 2006, AJ, 132, 2296
Arzoumanian, D., André, P., Didelon, P., et al. 2011, A&A, 529, L6
Bastian, N., Adamo, A., Gieles, M., et al. 2011, MNRAS, 417, L6
Bonatto, C., & Bica, E. 2011, MNRAS, 414, 3769
Bonnell, I. A., Bate, M. R., & Vine, S. G. 2003, MNRAS, 343, 413
Chandar, R., Whitmore, B. C., Calzetti, D., et al. 2011, ApJ, 727, 88

Drew, J. E., Busfield, G., Hoare, M. G., et al. 1997, MNRAS, 286, 538
Eisenstein, D. J., & Hut, P. 1998, ApJ, 498, 137
Fang, M., van Boekel, R., Wang, W., et al. 2009, A&A, 504, 461
Federrath, C. 2013a, MNRAS, 436, 1245
—. 2013b, MNRAS, 436, 3167
Federrath, C., & Klessen, R. S. 2013, ApJ, 763, 51
Federrath, C., Roman-Duval, J., Klessen, R. S., Schmidt, W., & Mac Low, M.-M. 2010, A&A, 512, A81

646, 1215

Figuerêdo, E., Blum, R. D., Damineli, A., & Conti, P. S. 2002, AJ, Flaherty, K. M., & Muzerolle, J. 2008, AJ, 135, 966 Fujii, M., Iwasawa, M., Funato, Y., & Makino, J. 2009, ApJ, 695, Fujii, M. S. 2015a, PASJ, 67, 59 —. 2015b, PASJ, arXiv:1410.5540 Fujii, M. S., & Portegies Zwart, S. 2013, MNRAS, 430, 1018 . 2014, MNRAS, 439, 1003 —. 2015, MNRAS, 449, 726 Fukui, Y., Ohama, A., Hanaoka, N., et al. 2013, ArXiv e-prints, arXiv:1306.2090 . 2014, ApJ, 780, 36 Furukawa, N., Dawson, J. R., Ohama, A., et al. 2009, ApJ, 696, L115 Gerritsen, J. P. E., & Icke, V. 1997, A&A, 325, 972 Gieles, M., Athanassoula, E., & Portegies Zwart, S. F. 2007, MNRAS, 376, 809 Gieles, M., Heggie, D. C., & Zhao, H. 2011, MNRAS, 413, 2509 Gieles, M., & Portegies Zwart, S. F. 2011, MNRAS, 410, L6 Girichidis, P., Federrath, C., Allison, R., Banerjee, R., & Klessen, R. S. 2012, MNRAS, 420, 3264 Girichidis, P., Federrath, C., Banerjee, R., & Klessen, R. S. 2011, MNRAS, 413, 2741 Gürkan, M. A., Freitag, M., & Rasio, F. A. 2004, ApJ, 604, 632 Heggie, D. C. 1975, MNRAS, 173, 729 Hénon, M. 1965, Annales d'Astrophysique, 28, 62 Hernquist, L., & Katz, N. 1989, ApJS, 70, 419 Heyer, M. H., & Brunt, C. M. 2004, ApJ, 615, L45 Higuchi, A. E., Kurono, Y., Saito, M., & Kawabe, R. 2009, ApJ, 705, Hodapp, K.-W., & Rayner, J. 1991, AJ, 102, 1108Holmberg, J., & Flynn, C. 2000, MNRAS, 313, 209 Horner, D. J., Lada, E. A., & Lada, C. J. 1997, AJ, 113, 1788 Hurley, J. R., Pols, O. R., & Tout, C. A. 2000, MNRAS, 315, 543 Hut, P. 1983, ApJ, 272, L29 Inoue, T., & Fukui, Y. 2013, ApJ, 774, L31 Kim, W.-T., & Ostriker, E. C. 2002, ApJ, 570, 132 King, I. R. 1966, AJ, 71, 64 Krumholz, M. R., Dekel, A., & McKee, C. F. 2012, ApJ, 745, 69 Krumholz, M. R., & McKee, C. F. 2005, ApJ, 630, 250 Lada, C. J., & Lada, E. A. 2003, ARA&A, 41, 57 Larson, R. B. 1981, MNRAS, 194, 809 Levine, J. L., Steinhauer, A., Elston, R. J., & Lada, E. A. 2006, ApJ,

Lynden-Bell, D., & Wood, R. 1968, MNRAS, 138, 495 Mac Low, M.-M., & Klessen, R. S. 2004, Reviews of Modern Physics, 76, 125
McKee, C. F., & Ostriker, E. C. 2007, ARA&A, 45, 565
Murray, N. 2011, ApJ, 729, 133
Nitadori, K., & Makino, J. 2008, New Astronomy, 13, 498
Ohama, A., Dawson, J. R., Furukawa, N., et al. 2010, ApJ, 709, 975
Ostriker, E. C., Stone, J. M., & Gammie, C. F. 2001, ApJ, 546, 980
Parmentier, G., & Pfalzner, S. 2013, A&A, 549, A132
Parmentier, G., Pfalzner, S., & Grebel, E. K. 2014, ApJ, 791, 132
Pelupessy, F. I. 2005, PhD thesis, Leiden Observatory, Leiden
University, P.O. Box 9513, 2300 RA Leiden, The Netherlands
Pelupessy, F. I., & Portegies Zwart, S. 2012, MNRAS, 420, 1503
Pelupessy, F. I., van der Werf, P. P., & Icke, V. 2004, A&A, 422, 55
Pelupessy, F. I., van Elteren, A., de Vries, N., et al. 2013, A&A, 557,
A84 76, 125 A84 Pfalzner, S. 2009, A&A, 498, L37 2011, A&A, 536, A90 Pfalzner, S., & Kaczmarek, T. 2013, A&A, 559, A38
Pfalzner, S., Parmentier, G., Steinhausen, M., Vincke, K., & Menten, K. 2014, ApJ, 794, 147 Piskunov, A. E., Kharchenko, N. V., Schilbach, E., et al. 2008, A&A, 487, 557 Portegies Zwart, S., McMillan, S. L. W., van Elteren, E., Pelupessy, I., & de Vries, N. 2013, Computer Physics Communications, 183, Portegies Zwart, S., McMillan, S., Harfst, S., et al. 2009, New A, 14, 369 Portegies Zwart, S. F., & McMillan, S. L. W. 2002, ApJ, 576, 899 Portegies Zwart, S. F., McMillan, S. L. W., & Gieles, M. 2010, ARA&A, 48, 431 Roman-Duval, J., Federrath, C., Brunt, C., et al. 2011, ApJ, 740, Salpeter, E. E. 1955, ApJ, 121, 161 Spitzer, L. 1987, Dynamical evolution of globular clusters Spitzer, L. J., & Hart, M. H. 1971, ApJ, 164, 399
Springel, V., & Hernquist, L. 2002, MNRAS, 333, 649
Winston, E., Megeath, S. T., Wolk, S. J., et al. 2009, AJ, 137, 4777
Wolff, S. C., Strom, S. E., Dror, D., & Venn, K. 2007, AJ, 133, 1092
Zinnecker, H., & Yorke, H. W. 2007, ARA&A, 45, 481

Luhman, K. L., Stauffer, J. R., Muench, A. A., et al. 2003, ApJ, 593,